

hep-ph/0001159

DSF-42/99

The Strange Quark Problem in the Framework of Statistical Distributions

F. Buccella, O. Pisanti, and L. Rosa

Dipartimento di Scienze Fisiche, Università di Napoli, Mostra d'Oltremare, Pad.19,
I-80125, Napoli, Italy;
INFN, Sezione di Napoli, Napoli, Italy.

Abstract

A large class of polarized and unpolarized deep inelastic data is successfully described with Fermi-Dirac functions for the non-diffractive part of quark parton distributions. The NLO approach used here improves the agreement with experiment of the previous LO work. We get a broader distribution for the strange parton $s(x)$ than for $\bar{s}(x)$.

PACS numbers: 13.60.-r, 13.60.Hb, 14.20.Dh

1 Introduction

The possibility of having $s(x) \neq \bar{s}(x)$ has been advocated [1] to explain the conflict between two different determinations of the strange quark sea in the nucleon. The CTEQ global analysis [2] obtained the strange quark distribution on the assumption of $s(x) = \bar{s}(x)$. Actually, the measured quantity was the following combination of nucleon structure functions on an isoscalar target, N :

$$\frac{5}{12} \left(F_2^{\nu N} + F_2^{\bar{\nu} N} \right) - 3 F_2^{\mu N} = \frac{x}{2} [s(x) + \bar{s}(x)], \quad (1)$$

where the sum of F_2 neutrino structure function came from CCFR DIS data from neutrino and antineutrino beams [3] and $F_2^{\mu N}$ from the NM Collaboration [4]. The result of this mean strange-antistrange quark distribution was found to be quite different from the strange quark distribution extracted from dimuon events of CCFR [5]. Since the neutrino events dominate the CCFR data set, one should consider the latter result as $s(x)$. Therefore one may consider the conflict as a first evidence for the difference between $s(x)$ and $\bar{s}(x)$. Note that as a result of the reanalysis by CCFR [6], including the effect of higher-order QCD corrections, the observed discrepancy is reduced, but it is still significant. An interesting contribution to this problem would be represented by an independent evidence of $s(x) \neq \bar{s}(x)$. New neutrino and antineutrino data on F_2 and F_3 have been measured [7] and they are quantities (especially F_3) sensitive to $s(x) \neq \bar{s}(x)$. Therefore a global analysis of nucleon structure functions, including F_2 and F_3 from neutrino and antineutrino beams rather than the dimuon events of CCFR measurement, may provide this kind of independent confirmation.

On the theoretical side, with the heuristic argument that $m_\Lambda/3 > m_K/2$ [1] a broader distribution for $s(x)$ (expected to combine with the valence u and d quarks to give a Λ) than for $\bar{s}(x)$ (expected to combine with the same quarks to give a K) was advocated. This is just the property that could explain the previously mentioned data conflict.

In another scenario, a different shape for $s(x)$ and $\bar{s}(x)$ may be naturally understood in the framework of an approach developed in the last years [8, 9, 10]. With the motivation of keeping into account the role played by Pauli principle in explaining several experimental facts, the parton distributions were described [9] in terms of the sum of a *gas* component, given by a Fermi-Dirac function for quarks ($i = u^\uparrow, u^\downarrow, d^\uparrow, d^\downarrow, \bar{u}, \bar{d}$),

$$p_{i,gas}(x) = \frac{A x^\alpha (1-x)^\beta}{\exp\left(\frac{x-\tilde{x}_i}{\bar{x}}\right) + 1}, \quad (2)$$

and a *liquid* term, unpolarized and isoscalar, given by

$$L(x) = 0.12 x^{-1.19} (1-x)^{9.6}. \quad (3)$$

For the gluons a Bose-Einstein function was taken ($i = g^\uparrow, g^\downarrow$),

$$p_{i,gas}(x) = \frac{8}{3} \frac{A x^\alpha (1-x)^\beta}{\exp\left(\frac{x-\tilde{x}_i}{\bar{x}}\right) - 1}. \quad (4)$$

In Eq.s (2) and (4) \bar{x} plays the role of a *temperature*, \tilde{x}_i of a *thermodynamic potential*, depending on the flavour and the spin of each parton, and the function in the numerator is a weight function for the density levels of the quarks in the $P_z = \infty$ frame of reference. In Ref. [9] this statistical parametrization was applied for describing both polarized and unpolarized data and compared with a standard one, obtaining a very good agreement between the first, second, and third moment of the distributions.

However, it is rather natural to assume different weight functions for q and \bar{q} , since in the nucleon, which is not a C invariant object, the quarks (transforming as a 3 under $SU(3)_c$) dominate over the antiquark (transforming as a $\bar{3}$). Indeed, inspired by the previously mentioned heuristic argument ($m_\Lambda/3 > m_K/2$), we expect a broader weight function for the quarks than for the antiquarks. The strange quark is the best one to test this idea, since it is the lightest not valence parton.

With respect to the analysis of Ref. [9], that was performed at Leading Order (LO) in the strong coupling, α_s , here we include the Next to Leading Order (NLO) corrections. We study a large class of polarized and unpolarized data within the framework just described, with the important modification of taking different weight functions for quarks and antiquarks.

The paper is organized as follows. In Section 2 the input parametrizations of the parton distributions are presented, Section 3 is devoted to the description of the experimental data used in our analysis and of the method of resolution of evolution equations, and Section 4 reports our results and conclusions.

2 Parton Parametrizations

According to the hypothesis of a role of Pauli principle for quark parton distributions, we take, at $Q_0^2 = 3 \text{ GeV}^2$, Fermi-Dirac functions for u and d quarks ($i = u^\uparrow, u^\downarrow, d^\uparrow, d^\downarrow$),

$$p_i(x, Q_0^2) = \frac{f_q(x)}{\exp\left(\frac{x-\tilde{x}_i}{\bar{x}}\right) + 1} + \frac{1}{2} f_L(x), \quad (5)$$

where the last term,

$$f_L(x) = A_L x^{\alpha_L} (1-x)^{\beta_L}, \quad (6)$$

represents an unpolarized and isoscalar part which takes into account the large diffractive contribution in the small x region ($-2 < \alpha_L \leq -1$).

With the aim of allowing different shapes for $s(x)$ and $\bar{s}(x)$, we take a different form for the weight function of antiquarks. Since at small x the single parton contribution is overwhelmed by the diffractive one, it is very difficult to determine the difference in the exponents of x . So, we assume them equal for quarks and antiquarks, allowing, instead, different values for the exponents of $(1-x)$, which is sensitive to the large x behaviour where the diffractive contribution becomes negligible. In conclusion we have

$$f_q(x) = A_q x^\alpha (1-x)^{\beta_q}, \quad (7)$$

$$f_{\bar{q}}(x) = A_{\bar{q}} x^\alpha (1-x)^{\beta_{\bar{q}}}, \quad (8)$$

with $\alpha > -1$.

In the analysis of Ref. [9] we found rather negative values for the *potentials* of the partons in the sea, which correspond to the Boltzmann limit for their distributions. We then parametrize s , \bar{u} , and \bar{d} in the following way:

$$\bar{u}(x, Q_0^2) = k_{\bar{u}} f_{\bar{q}}(x) e^{-\frac{x}{\bar{x}}} + f_L(x), \quad (9)$$

$$\bar{d}(x, Q_0^2) = k_{\bar{d}} f_{\bar{q}}(x) e^{-\frac{x}{\bar{x}}} + f_L(x), \quad (10)$$

$$s(x, Q_0^2) = k_s f_q(x) e^{-\frac{x}{\bar{x}}} + \frac{2}{4.2} f_L(x). \quad (11)$$

Note that the different coefficient in front of $f_L(x)$ in Eq. (11) takes into account the results of Ref. [6] in the relative size of the strange sea with respect to the non-strange one. This result is also used to decrease the number of parameters, in writing

$$\bar{s}(x, Q_0^2) = \frac{\bar{u}(x, Q_0^2) + \bar{d}(x, Q_0^2)}{4.2}, \quad (12)$$

with, however, the requirement that the first moments of s and \bar{s} be equal, since the nucleons have no strangeness.

The defect in the Gottfried sum rule [11] implies a non trivial sea in the nucleons, with $\bar{d} > \bar{u}$, as confirmed also by the experiments NA51 at CERN [12] and E866 at FNAL [13]. Along this line, we should also consider the possibility of polarization in the quark sea, as advocated to account for the large defect in the Ellis and Jaffe sum rule [14] for the polarized structure function of the proton, g_1^p , first shown in the EMC experiment [15] and confirmed by the following ones. We expect the distributions to be proportional to the *gas* component of the unpolarized ones,

$$\Delta \bar{u}(x, Q_0^2) = \Delta k_{\bar{u}} [\bar{u}(x, Q_0^2) - f_L(x)], \quad (13)$$

$$\Delta \bar{d}(x, Q_0^2) = \Delta k_{\bar{d}} [\bar{d}(x, Q_0^2) - f_L(x)], \quad (14)$$

$$\Delta s(x, Q_0^2) + \Delta \bar{s}(x, Q_0^2) = \Delta k_{s\bar{s}} \left[s(x, Q_0^2) + \bar{s}(x, Q_0^2) - \frac{4}{4.2} f_L(x) \right], \quad (15)$$

with $|\Delta k_i| \leq 1$ and for simplicity we have taken the same proportionality constant for s and \bar{s} . The isovector combination $\Delta \bar{u} - \Delta \bar{d}$ is thus proportional to the *gas* component of $\bar{u} + \bar{d}$ by a

factor, which is less than one in modulus for the positivity constraints on polarized distributions, and reaches that value only in the extreme cases of full and opposite polarization for \bar{u} and \bar{d} . For the isoscalar combination we have a part proportional to $f_{\bar{q}}$, $\Delta\bar{u} + \Delta\bar{d}$ and $\Delta\bar{s}$, and another one, Δs , proportional to f_q . In conclusion, we have three parameters, $\Delta k_{\bar{u}}$, $\Delta k_{\bar{d}}$, and $\Delta k_{s\bar{s}}$ to describe the sea contribution to the two polarized structure functions of the nucleons, g_1^p and g_1^n .

For the gluon distribution we take the Bose-Einstein form ($i = g^\uparrow, g^\downarrow$),

$$p_i(x, Q_0^2) = \frac{f_g(x)}{\exp\left(\frac{x-\tilde{x}_i}{\tilde{x}}\right) - 1}, \quad (16)$$

with f_g given by

$$f_g(x) = \frac{8}{3} A_g x^{\alpha_g} (1-x)^{\beta_g}, \quad (17)$$

but with the constraint $\alpha_g \leq \alpha$. Note that a more divergent term, similar to the second one in the r.h.s. of Eq. (5), seems to be excluded by data; so, we chose not to include it in Eq. (16).

We impose that the total momentum of the partons be unity. Other constraints on the distributions concern the values of the following unpolarized sum rules:

$$I_{Adler} = 1.01 \pm 0.20, \quad (18)$$

$$I_{GLS} = 2.5 \pm 0.08, \quad (19)$$

$$I_{Gottfried} = 0.235 \pm 0.026. \quad (20)$$

As far as the Adler sum rule [16] is concerned, we consider this constraint as an exact one, while we use the experimental errors for the other ones. Moreover, in calculating the theoretical value of the Gross-Llewellyn-Smith sum rule [17] we include the QCD corrections up to $O(\alpha_s^3)$ [18],

$$I_{GLS}(Q^2) = I_{GLS}^{(0)}(Q^2) \left[1 - \frac{\alpha_s(Q^2)}{\pi} - 3.25 \left(\frac{\alpha_s(Q^2)}{\pi} \right)^2 - 12.20 \left(\frac{\alpha_s(Q^2)}{\pi} \right)^3 \right], \quad (21)$$

where

$$I_{GLS}^{(0)}(Q^2) = \int_0^1 dx [u - \bar{u} + d - \bar{d} + s - \bar{s}](x, Q^2). \quad (22)$$

Finally, we constrain the ratio $(\bar{u}/\bar{d})(x = 0.18)$ to the value 0.51 ± 0.06 measured by the experiment NA51 [12].

3 Description of Data and Parton Evolution

We perform a NLO description, in the \overline{MS} scheme, of the unpolarized data on F_2^ν and F_3^ν from CCFR [7], $F_2^{p,d}$ from NMC [19], and of the polarized structure functions measured at SLAC in

the E142 [20], E143 [21], and E154 [22] experiments, at HERA in the HERMES experiment [23], and at CERN in the SMC experiment [24]. All the unpolarized data were subjected to the cuts $Q^2 \geq 2 \text{ GeV}^2$ and $W^2 \geq 10 \text{ GeV}^2$. We add a 1.5% uncertainty to the statistical errors of CCFR data since no global systematic errors are given.

For solving the DGLAP evolution equations [25] we use the Jacobi polynomial method [26], which some of us already used in an analysis of polarized structure functions [27]. Here, we briefly recall the procedure. The given structure function is expressed in terms of a truncated series of Jacobi polynomials, $\Theta_k^{\alpha\beta}(x)$,

$$F(x, Q^2) = x^\alpha (1-x)^\beta \sum_{k=0}^N a_k^{(\alpha\beta)}(Q^2) \Theta_k^{\alpha\beta}(x), \quad (23)$$

where $\Theta_k^{\alpha\beta}$ satisfy the orthogonality condition

$$\int_0^1 x^\alpha (1-x)^\beta \Theta_k^{\alpha\beta} \Theta_l^{\alpha\beta} dx = \delta_{kl}. \quad (24)$$

By using the definition of the coefficients, $a_k^{(\alpha\beta)}$,

$$a_k^{(\alpha\beta)}(Q^2) = \int_0^1 F(x, Q^2) \Theta_k^{\alpha\beta}(x) dx, \quad (25)$$

with a little algebra it is possible to obtain for $F(x, Q^2)$ the following expression,

$$F(x, Q^2) = x^\alpha (1-x)^\beta \sum_{k=0}^N \Theta_k^{\alpha\beta}(x) \sum_{j=0}^k c_j^{(k)}(\alpha, \beta) F_{j+1}(Q^2), \quad (26)$$

where $c_j^{(k)}(\alpha, \beta)$ are the coefficients of the expansion of the Jacobi polynomials, $\Theta_k^{\alpha\beta}(x)$, in power of x , and $F_n(Q^2)$ are the Mellin moments of $F(x, Q^2)$,

$$F_n(Q^2) = \int_0^1 x^{n-1} F(x, Q^2) dx. \quad (27)$$

In this way, the Q^2 dependence of $F(x, Q^2)$ is factorized in its moments, for which the solution of the evolution equations up to NLO is well known.

In this analysis we reconstructed the unpolarized structure functions with $N = 12$ and the polarized ones with $N = 9$. Moreover, we used different values of α and β for the different data sets. Table 1 reports the values of the parameters which give the best convergence of the Jacobi expansion.

The unpolarized parton distributions at Q_0^2 are combined to give the following non-singlet (Q_i), singlet (Σ) and gluon terms (G) (we suppress for brevity the x and Q_0^2 dependence of the

various terms),

$$Q_p = 2(u + \bar{u}) - (d + \bar{d}) - (s + \bar{s}), \quad (28)$$

$$Q_n = 2(d + \bar{d}) - (u + \bar{u}) - (s + \bar{s}), \quad (29)$$

$$Q_3 = u - \bar{u} + d - \bar{d} + s - \bar{s}, \quad (30)$$

$$Q_s = s - \bar{s}, \quad (31)$$

$$\Sigma = u + \bar{u} + d + \bar{d} + s + \bar{s}, \quad (32)$$

$$G = g, \quad (33)$$

while in the polarized case we have

$$\delta Q_p = a_3 + \frac{a_8}{3} = \frac{4}{3}(\Delta u + \Delta \bar{u}) - \frac{2}{3}(\Delta d + \Delta \bar{d} + \Delta s + \Delta \bar{s}), \quad (34)$$

$$\delta Q_n = -a_3 + \frac{a_8}{3} = \frac{4}{3}(\Delta d + \Delta \bar{d}) - \frac{2}{3}(\Delta u + \Delta \bar{u} + \Delta s + \Delta \bar{s}), \quad (35)$$

$$\delta \Sigma = a_0 = \Delta u + \Delta \bar{u} + \Delta d + \Delta \bar{d} + \Delta s + \Delta \bar{s}, \quad (36)$$

$$\delta G = \Delta g. \quad (37)$$

The moments of the previous quantities at Q_0^2 are evolved to the Q^2 of data (see [27] for the complete expressions of the evolved moments). The relation between the evolved moments of the combinations in Eq.s (28)-(37) and the structure function moments, to be used in Eq. (26), comes from the expression of the unpolarized and polarized structure functions. Neglecting for the moment the charm contribution, we have for the first ones (for neutrino structure functions we give the expressions for isoscalar targets)

$$\frac{F_2^{ep}(x, Q^2)}{x} = \left\{ C_2^q \otimes \left(\frac{1}{9} Q_p + \frac{2}{9} \Sigma \right) \right\} (x, Q^2) + (C_2^g \otimes G)(x, Q^2), \quad (38)$$

$$\frac{F_2^{en}(x, Q^2)}{x} = \left\{ C_2^q \otimes \left(\frac{1}{9} Q_n + \frac{2}{9} \Sigma \right) \right\} (x, Q^2) + (C_2^g \otimes G)(x, Q^2), \quad (39)$$

$$F_2^{ed}(x, Q^2) = \frac{1}{2} (F_2^{ep}(x, Q^2) + F_2^{en}(x, Q^2)), \quad (40)$$

$$\begin{aligned} \frac{F_2^{CCFR}(x, Q^2)}{x} &= \frac{1}{x} \left[F_2^{(\nu+\bar{\nu})} + (2\alpha - 1) F_2^{(\nu-\bar{\nu})} \right] = \left\{ C_2^q \otimes \left[\frac{1 + |V_{ud}|^2}{6} (2\Sigma + Q_p + Q_n) + \right. \right. \\ &\quad \left. \left. \frac{|V_{us}|^2}{3} (\Sigma - Q_p - Q_n) + (2\alpha - 1) \left(\frac{-|V_{us}|^2}{2} (Q_3 - Q_s) + |V_{us}|^2 Q_s \right) \right] \right\} (x, Q^2) + \\ &\quad (C_2^g \otimes G)(x, Q^2), \end{aligned} \quad (41)$$

$$F_3^{CCFR}(x, Q^2) = F_3^{(\nu+\bar{\nu})} = \left\{ C_3^q \otimes \left[\frac{1 + |V_{ud}|^2}{2} (Q_3 - Q_s) + |V_{us}|^2 Q_s \right] \right\} (x, Q^2). \quad (42)$$

In the previous equations C_i^q and C_2^g are the coefficient functions for quarks and gluons, which at LO are given by

$$C_i^q(x) = \delta(1 - x), \quad C_2^g(x) = 0, \quad (43)$$

and at NLO can be found, for example, in [28]. The convolution \otimes is defined as

$$(f \otimes g)(x) \equiv \int_x^1 \frac{dz}{z} f\left(\frac{x}{z}\right) g(z) = \int_x^1 \frac{dz}{z} f(z) g\left(\frac{x}{z}\right). \quad (44)$$

In the neutrino structure function the Cabibbo-Kobayashi-Maskawa [29] elements appear, for which we use the following values: $|V_{ud}|^2 = 0.9508$, $|V_{us}|^2 = 1 - |V_{ud}|^2$, $|V_{cd}|^2 = 0.0488$, $|V_{cs}|^2 = 0.9493$. Moreover, $\alpha = 0.828$ is the fraction of ν with respect to $\bar{\nu}$ in the CCFR experiment [30] and a term with α in the r.h.s. of Eq. (42) does not appear since the CCFR data have already been corrected for the $s + \bar{s}$ contribution [7]. The polarized structure functions are

$$g_1^{p,n}(x) = \frac{1}{12} \left[(\delta C^q \otimes \delta Q_{p,n})(x, Q^2) + \frac{4}{3} (\delta C^g \otimes \delta \Sigma)(x, Q^2) \right], \quad (45)$$

$$g_1^d(x) = \frac{1}{2} \left(1 - \frac{3}{2} \omega_D \right) [g_1^p(x) + g_1^n(x)], \quad (46)$$

where δC^i are the polarized coefficient functions for quarks and gluons (see, for example, [31] for their expression) and $\omega_D = 0.058$ [32] is the D-wave component in the deuteron ground state. Note, however, that, when experimentally available, we fit the asymmetries

$$A_1^{p,n}(x, Q^2) = \frac{g_1^{p,n}(x, Q^2)}{F_1^{p,n}(x, Q^2)} = \frac{g_1^{p,n}(x, Q^2)}{F_2^{p,n}(x, Q^2)} 2x (1 + R^{p,n}(x, Q^2)), \quad (47)$$

with $R = F_L/(2x F_1)$.

As stressed in [33], a consistent treatment of heavy flavours can be carried out in the Fixed Flavour Scheme (FFS), where the heavy quarks are not considered as intrinsic partons, but produced by the interactions of the other partons (light quarks and gluons). To this aim, we fix the number of active flavours in the splitting functions to be 3 and add the charm contributions to neutral and charged current F_2 and $x F_3$ (we neglect the small b quark contribution and the c contribution to the polarized structure function g_1),

$$F_{2_{NC}}^{(c)}(x, Q^2) = e_c^2 \frac{\hat{\alpha}_s}{\pi} x \int_{\xi}^1 \frac{dy}{y} \hat{C}_2^{g(c)}\left(\frac{x}{y}, Q^2\right) \hat{G}(y), \quad (48)$$

$$F_{2_{CC}}^{(c)}(x, Q^2) = 2 \xi \hat{q}'(\xi) + \frac{\hat{\alpha}_s}{\pi} \xi \sum_{p=q',g} \int_{\xi}^1 \frac{dy}{y} \hat{H}_2^p\left(\frac{\xi}{y}, Q^2\right) \hat{p}(y), \quad (49)$$

$$F_3^{(c)}(x, Q^2) = 2 \hat{q}'(\xi) + \frac{\hat{\alpha}_s}{\pi} \sum_{p=q',g} \int_{\xi}^1 \frac{dy}{y} \hat{H}_3^p\left(\frac{\xi}{y}, Q^2\right) \hat{p}(y). \quad (50)$$

In the previous equations the hat indicates that we are calculating a quantity at $Q^2 = \mu^2$ and

$$\hat{C}(x, Q^2) \equiv C(x, Q^2, \mu^2), \quad \hat{H}(x, Q^2) \equiv H(x, Q^2, \mu^2), \quad (51)$$

where μ is the factorization scale, equal to $4 m_c^2$ and $Q^2 + m_c^2$ in the neutral and charged current processes, respectively; the expressions of the C and H 's can be found, for example, in [34] and

[35]; $\xi(x, Q^2) = x \ a(Q^2)$, where

$$a(Q^2) = \begin{cases} 1 + \frac{4 m_c^2}{Q^2}, & \text{for NC,} \\ 1 + \frac{m_c^2}{Q^2}, & \text{for CC.} \end{cases} \quad (52)$$

Furthermore, in Eqs (49) and (50) we have

$$q' = \begin{cases} \frac{1}{2} \left[\frac{|V_{cd}|^2}{6} (2 \Sigma + Q_p + Q_n) + \frac{|V_{cs}|^2}{3} (\Sigma - Q_p - Q_n) \right], & \text{for } F_2^{\nu+\bar{\nu}}, \\ \frac{1}{2} \left[\frac{|V_{cd}|^2}{2} (Q_3 - Q_s) + |V_{cs}|^2 Q_s \right], & \text{for } F_2^{\nu-\bar{\nu}}, \\ \frac{1}{2} \left[\frac{|V_{cd}|^2}{2} (Q_3 - Q_s) + |V_{cs}|^2 Q_s \right], & \text{for } F_3. \end{cases} \quad (53)$$

Differently from the charm quark treatment, in the expression of the QCD coupling constant, we include the usual active flavours, n_f , below each threshold,

$$\begin{aligned} \frac{\alpha_s^{NLO}(Q^2)}{4\pi} &= \frac{1}{\beta_0 \ln \frac{Q^2}{\Lambda^2}} - \frac{\beta_1}{\beta_0^3} \frac{\ln \ln \frac{Q^2}{\Lambda^2}}{\ln^2 \frac{Q^2}{\Lambda^2}}, \\ \beta_0 &= 11 - \frac{2}{3} n_f, \quad \beta_1 = 102 - \frac{38}{3} n_f, \end{aligned} \quad (54)$$

where $\Lambda_{NLO}^{(5)}$ is fixed to the value 0.2263, so to have $\alpha_s(M_Z^2) = 0.118$ [36]. Whenever is necessary we use the following values for the heavy quark masses:

$$m_c = 1.5 \text{ GeV}, \quad m_b = 4.5 \text{ GeV}. \quad (55)$$

4 Results and Conclusions

We consider the three following cases:

Fit 1: $\Delta\bar{u}, \Delta\bar{d}, \Delta s + \Delta\bar{s} \neq 0$

Fit 2: $\Delta\bar{u}, \Delta\bar{d} \neq 0, \Delta s + \Delta\bar{s} = 0$

Fit 3: $\Delta\bar{u} = \Delta\bar{d} = 0, \Delta s + \Delta\bar{s} \neq 0$

In Table 2 the values of the parameters for Fit 1 are reported. We do not show the results for Fits 2 and 3 because they look very similar to Fit 1 in the parameter values and χ^2_{red} (1.76 and 1.80, respectively), with a very small difference in the gluon contribution, which results in a negligible positive polarization ($\Delta g = 0.058$) for Fit 2 and a slightly larger one ($\Delta g = 0.113$) for Fit 3. Table 3 shows the comparison between the polarization of antiquarks in Fit 1, 2,

and 3. Interestingly enough, \bar{u} in Fit 2 and $s + \bar{s}$ in Fit 3 come out fully negative polarized to confirm that, as supposed in the interpretation of the EMC result in the gauge-invariant factorization schemes, the sea is negatively polarized. It is however difficult to disentangle the sea contribution to the polarization from the valence one, especially since sea partons are mostly present at small x , where the large diffractive contribution makes more unprecise the determination of the polarized structure functions. Indeed, one has to find the polarized cross-section, which is expected to vanish in the limit $x \rightarrow 0$, from the difference of two cross-sections, which go to infinity in the same limit. The values of $a_8 \equiv \Delta u + \Delta \bar{u} + \Delta d + \Delta \bar{d} - 2(\Delta s + \Delta \bar{s})$, which are related from $SU(3)$ symmetry to the combination $3F - D = 0.579 \pm 0.025$ [37], are very different for Fit 2 (0.373) and 3 (0.884), while Fit 1 is similar to Fit 3 (0.956). This shows that at the moment we cannot provide a test for this $SU(3)$ prediction.

In Table 3 the values of the polarized sum rules, Bjorken [38], Ellis-Jaffe [14] for the proton and for the neutron, are also reported in correspondence of the three considered cases. The values for the Bjorken sum rule are consistent with the $O(\alpha_s^3)$ theoretical prediction at $Q^2 = 3 \text{ GeV}^2$, 0.174 ± 0.002 .

The quark distributions at Q_0^2 are plotted in Fig. 1. In Fig. 2 we compare Q_p , Q_n , Σ , and g , evolved to $Q^2 = 1 \text{ GeV}^2$, with the same quantities obtained from the global fit of Ref. [39]. Note, however, that in Ref. [39] a different prescription [40] for the charm quark treatment, instead of the FFS, was used* and the value $m_c = 1.35 \text{ GeV}$. Fig.s 3-13 show the comparison with experimental data of the structure functions calculated for the values of parameters of Fit 1 (solid lines). We get a very good description of polarized data, which, however, have larger errors than the unpolarized ones. As far as the latter are concerned, a similar good quality is exhibited by the neutrino structure function $x F_3$, while the description of F_2^ν is not so accurate at low x . To some extent this can be observed for the high- x description of F_2^p and F_2^d too. Note, however, that if the CCFR data are not included in the analysis, the high- x behaviour of F_2^p and F_2^d drastically improves ($\chi^2_{red} = 0.97$ for the values of parameters reported in Table 2 as Fit 1a), as is evident from the comparison with data of the dashed lines in the figures. On one side, this suggests that, even with our hypothesis on strange quarks, the discrepancy between NMC neutral current data and CCFR charge current ones remains unresolved, and one has to consider other effects like charge asymmetry [1, 30]. On the other side, the high- x difference between solid and dashed lines in Fig. 3 and 4 is also justified by the fact that if the experimental ratio between F_2^p and $x F_3$ at high- x is different from 4/9 (the value implied by the dominance of u^\uparrow in that region) one cannot describe in a fully satisfactory way both the structure functions unless allowing more freedom in the quark parametrizations.

With respect to the results found in our previous LO analysis [9] we can confirm the pattern

*Actually, in Ref. [39] a variant of the ACOT scheme [41] was implemented. See Ref. [42] for an extensive review on this issue.

of the ratios $p_i^{(2)}/p_i^{(1)}$ between the second and the first moments of the *gas* component of the distributions of u^\uparrow , u^\downarrow , d^\uparrow , and d^\downarrow quarks, and we get similar values for the *temperature*, \bar{x} . Moreover, in agreement with the conclusions by Brodsky and Ma [1], we find a broader s distribution than \bar{s} , as shown by the higher value of the second moment of s with respect to \bar{s} . More precisely, we have for Fit 1 (similar values result for Fit 2 and 3)

$$p^{(2)} + \frac{2}{4.2} p_L^{(2)} = \begin{cases} 0.0421 & \text{for } s, \\ 0.0395 & \text{for } \bar{s}, \end{cases} \quad (56)$$

($p_L^{(2)}$ is the second moment of the *liquid* component) with a relative difference of $\sim 7\%$, compared to the value of 10% obtained in [1].

Finally, we can conclude that the fact that with the present NLO analysis we find $\chi_{red}^2 < 2$ (and < 1 for Fit 1a), which is smaller than the value found in our previous approach [9], is a good point in favour of statistical distributions.

Acknowledgments

We thank Bo-Qiang Ma for stimulating our interest in studying the strange parton distribution and for valuable and interesting observations.

REFERENCES

- [1] S.J. Brodsky and B.-Q. Ma, Phys. Lett. **B 381** (1996) 317.
- [2] CTEQ Collab., J. Botts *et al.*, Phys. Lett. **B304** (1993) 159.
- [3] CCFR Collab., S.R. Mishra *et al.*, Nevis Report 1459; W.C. Leung *et al.*, Phys. Lett. **B317** (1993) 655; P.Z. Quintas *et al.*, Phys. Rev. Lett. **71** (1993) 1307.
- [4] NM Collab., P. Amaudruz *et al.*, Phys. Lett. **B295** (1992) 159.
- [5] CCFR Collab., S.A. Rabinowitz *et al.*, Phys. Rev. Lett. **70** (1993) 134.
- [6] CCFR Collab., A.O. Bazarko *et al.*, Z. Phys. **C65** (1995) 189.
- [7] W.G. Seligman *et al.*, Phys. Rev. Lett. **79** (1997) 1213; W. Seligman, Ph.D. Thesis (Columbia University), Nevis Report 292.
- [8] F. Buccella and J. Soffer, Mod. Phys. Lett. **A8** (1993) 225; F. Buccella and J. Soffer, Europhys. Lett. **24** (1993) 165.

- [9] F. Buccella, I. Doršner, O. Pisanti, L. Rosa, and P. Santorelli, Mod. Phys. Lett. **A13** (1998) 441.
- [10] See also R.S. Bhalerao, N.G. Kelkar, and B. Ram, hep-ph/9911286, for an other recent example of statistical parametrization.
- [11] K. Gottfried, Phys. Rev. Lett. **18** (1967) 1154.
- [12] NA51 Collaboration, A. Baldit *et al.*, Phys. Lett. **B332** (1994) 244.
- [13] E866-NuSea Collab., E.A. Hawker *et al.*, Phys. Rev. Lett. **80** (1998) 3715; J.C. Peng *et al.*, Phys. Rev. **D58** (1998) 092004.
- [14] J. Ellis and R.L. Jaffe, Phys. Rev. **D9** (1974) 1444; *Erratum*, Phys. Rev. **D10** (1974) 1669.
- [15] EMC Collaboration, J. Ashman *et al.*, Phys. Lett. **B206** (1988) 364; Nucl. Phys. **B328** (1989) 1.
- [16] S.L. Adler, Phys. Rev. **143** (1966) 1144.
- [17] D.J. Gross and C.H. Llewellyn Smith, Nucl. Phys. **B14** (1969) 337.
- [18] S.A. Larin and J.A.M. Vermaseren, Phys. Lett. **B259** (1991) 345.
- [19] NM Collab., M. Arneodo *et al.*, Nucl. Phys. **B483** (1997) 3.
- [20] SLAC-E142 experiment, P. L. Anthony *et al.*, Phys. Rev. Lett. **71** (1993) 959; Phys. Rev. **D54** (1996) 6620.
- [21] SLAC-E143 experiment, K. Abe *et al.*, Phys. Rev. Lett. **74** (1995) 346; Phys. Rev. Lett. **75** (1995) 25; Phys. Lett. **B364** (1995) 61.
- [22] SLAC-E154 experiment, K. Abe *et al.*, Phys. Rev. Lett. **79** (1997) 26.
- [23] HERMES Collaboration: K. Ackerstaff *et al.*, Phys. Lett. **B404** (1997) 383.
- [24] SM Collab., B. Adeva *et al.*, Phys. Lett. **B412** (1997) 414; Phys. Rev. **D56** (1997) 5330; Phys. Lett. **B396** (1997) 338.
- [25] G. Altarelli and G. Parisi, Nucl. Phys. **B126** (1977) 298; Yu.L. Dokshitzer, D.I. Dyakonov, and S.I. Troyan, Phys. Lett. **B78** (1978) 290; Phys. Rep. **58** (1980) 269; V.N. Gribov and L.N. Lipatov, Sov. J. Nucl. Phys. **15** (1972) 438.
- [26] G. Parisi and N. Sourlas, Nucl. Phys. **B151** (1979) 421; I.S. Barker, C.B. Langensiepen, and G. Shaw, Nucl. Phys. **B186** (1981) 61; V.G. Krivokhizhin, S.P. Kurlovich, V.V. Sanadze, I.A. Savin, A.V. Sidorov, and N.B. Skachkov, Z. Phys. **C36** (1987) 51; V.G. Krivokhizhin, S.P. Kurlovich, V.V. Sanadze, I.A. Savin, A.V. Sidorov, and N.B. Skachkov, Z. Phys. **C48** (1990) 347.

- [27] C. Bourrely, F. Buccella, O. Pisanti, P. Santorelli, and J. Soffer, *Prog. Theor. Phys.* **99** (1998) 1017.
- [28] A. J. Buras, *Rev. Mod. Phys.* **52** (1980) 199.
- [29] N. Cabibbo, *Phys. Rev. Lett.* **10** (1963) 531; M. Kobayashi and T. Maskawa, *Prog. Theor. Phys.* **49 n.2** (1973) 652.
- [30] C. Boros, J.T. Londergan, and A.W. Thomas, *Phys. Rev. Lett.* **81** (1998) 4075; *Phys. Rev. D* **59** (1999) 074021.
- [31] M. Glück, E. Reya, M. Stratmann, and W. Vogelsang, *Phys. Rev. D* **53** (1996) 4775.
- [32] M. Lacombe *et al.*, *Phys. Lett.* **B101** (1981) 139.
- [33] M. Glück, E. Hoffmann, and E. Reya, *Z. Phys.* **C13** (1982) 119; M. Glück, R.M. Godbole, and E. Reya, *Z. Phys.* **C38** (1988) 441; M. Glück, E. Reya, and M. Stratmann, *Nuc. Phys.* **B422** (1994) 37.
- [34] M. Glück, E. Reya, and A. Vogt, *Z. Phys.* **C67** (1995) 433.
- [35] M. Glück, S. Kretzer, and E. Reya, *Phys. Lett.* **B380** (1996) 171; *Erratum*, *Phys. Lett. B* **405** (1997) 391.
- [36] Particle Data Group, R.M. Barnett *et al.*, *Phys. Rev. D* **54** (1996) 1.
- [37] F.E. Close and R.G. Roberts, *Phys. Lett.* **B313** (1993) 165.
- [38] J.D. Bjorken, *Phys. Rev.* **148** (1966) 1467; *Phys. Rev. D* **1** (1970) 1376.
- [39] A.D. Martin, R.G. Roberts, W.J. Stirling, R.S. Thorne, *Eur. Phys. J.* **C4** (1998) 463.
- [40] R.S. Thorne and R.G. Roberts, *Phys. Rev. D* **57** (1998) 6871.
- [41] M.A.G. Aivazis, J.C. Collins, F.I. Olness, and W.-K. Tung, *Phys. Rev. D* **50** (1994) 3102.
- [42] J.C. Collins, *Phys. Rev. D* **58** (1998) 094002.

	α	β
F_{NMC}	-0.078	0.077
F_{CCFR}	-0.99	0.500
F_c^{NC}	-0.096	1.210
F_c^{CC}	-0.096	1.210
F_1	-0.503	0.006
g_1	1.084	3.550

Table 1: Values of α and β in the Jacobi description of the structure functions relative to the NMC and CCFR experiments, to the charm component in neutral and charge current processes, and to F_1 and g_1 , respectively.

	Fit 1			Fit 1a		
χ^2_{red}	1.76			0.97		
$f_q(x)$	$3.55 x^{-0.275} (1-x)^{2.76}$			$3.34 x^{-0.254} (1-x)^{2.62}$		
$f\bar{q}(x)$	$7.33 x^{-0.275} (1-x)^{4.84}$			$8.28 x^{-0.254} (1-x)^{11.2}$		
$f_g(x)$	$87.4 x^{-0.276} (1-x)^{7.36}$			$88.0 x^{-0.255} (1-x)^{8.57}$		
$f_L(x)$	$0.124 x^{-1.14} (1-x)^{14.7}$			$0.120 x^{-1.15} (1-x)^{12.6}$		
\bar{x}	0.250			0.257		
ΔG	-0.009			-0.193		
	\tilde{x}_i	$p_i^{(1)}$	$p_i^{(2)}/p_i^{(1)}$	\tilde{x}_i	$p_i^{(1)}$	$p_i^{(2)}/p_i^{(1)}$
u^\uparrow	0.750	1.58	0.149	0.867	1.50	0.161
d^\downarrow	0.150	0.870	0.118	0.184	0.836	0.126
u^\downarrow	-0.033	0.581	0.109	0.047	0.639	0.119
d^\uparrow	-0.136	0.440	0.105	-0.100	0.447	0.113
g^\uparrow	-0.427	3.88	0.055	-0.409	3.93	0.052
g^\downarrow	-0.426	3.89	0.055	-0.399	4.12	0.052
	k_i			k_i		
\bar{u}	0.099	0.181	0.073	0.118	0.155	0.045
\bar{d}	0.181	0.330	0.073	0.232	0.303	0.045
\bar{s}	-	0.122	0.073	-	0.109	0.045

Table 2: Values of the parameters of the input distributions for Fit 1 and Fit 1a (see text). We denote the first and second moments of the *gas* component of the distributions with $p_i^{(1)}$ and $p_i^{(2)}$, respectively.

	Fit 1			Fit 2			Fit 3		
	Δk_i	$p_i^{(1)}$	$p_i^{(2)}$	Δk_i	$p_i^{(1)}$	$p_i^{(2)}$	Δk_i	$p_i^{(1)}$	$p_i^{(2)}$
$\Delta \bar{u}$	-1.00	-0.181	-0.013	-1.00	-0.185	-0.013	-	-	-
$\Delta \bar{d}$	0.24	0.080	0.006	0.50	0.017	0.001	-	-	-
$\Delta s + \Delta \bar{s}$	-1.00	-0.243	-0.020	-	-	-	-1.00	-0.208	-0.018
a_8	0.956			0.373			0.884		
Bj	0.174			0.175			0.176		
EJp	0.133			0.134			0.136		
EJn	-0.041			-0.041			-0.040		

Table 3: Values of the polarization parameters and sum rules for the three cases considered in the analysis.

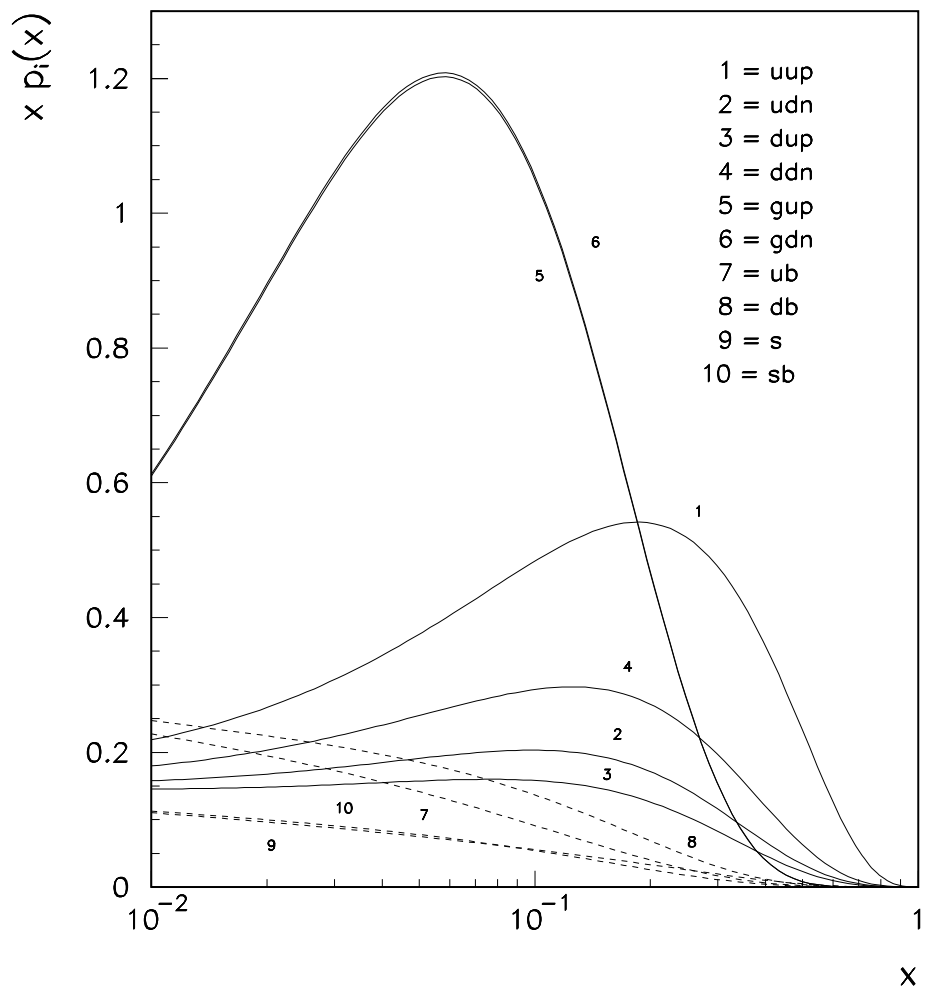


Figure 1: Quark and gluon distributions at $Q_0^2 = 3 \text{ GeV}^2$ for the values of parameters of Fit 1.

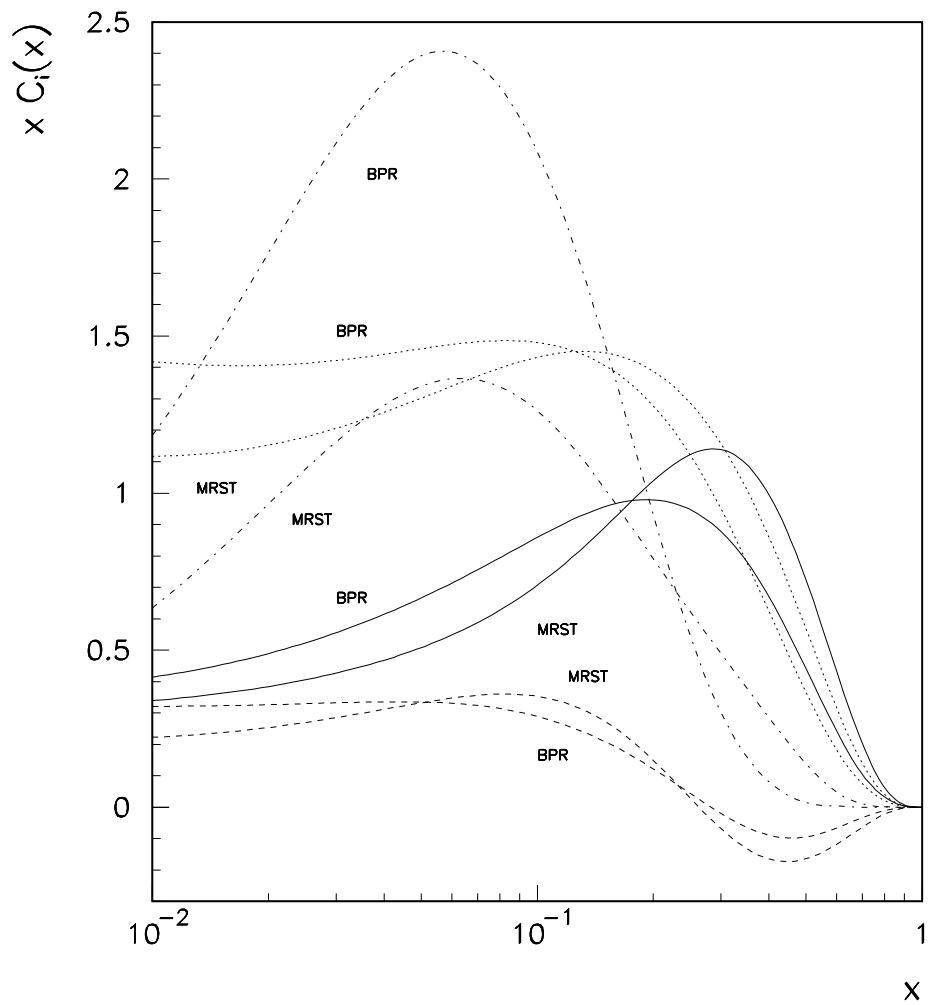


Figure 2: Comparison of Q_p (solid lines), Q_n (dashed lines), Σ (dotted lines), and g (dash-dotted lines), evolved to $Q^2 = 1 \text{ GeV}^2$ (BPR), with the same quantities obtained from the fit of Ref. [39] (MRST).

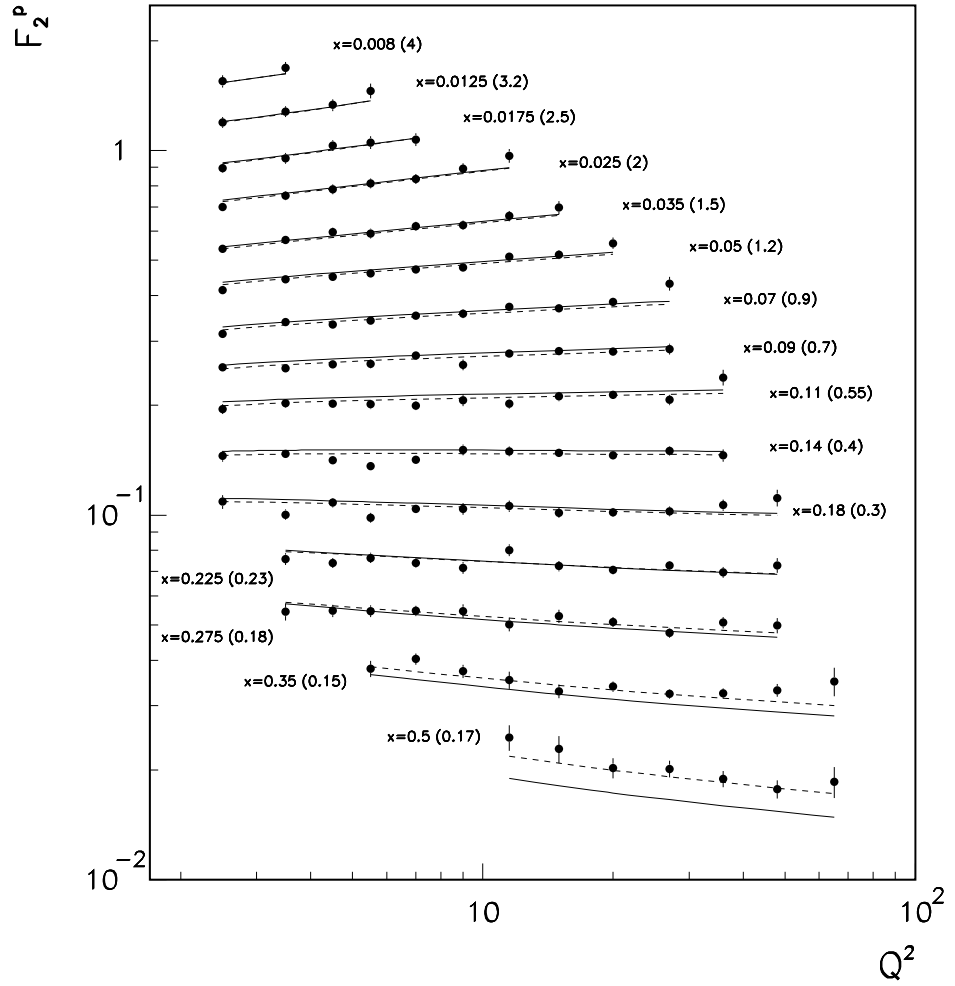


Figure 3: Comparison of the prediction of the fit with the experimental data on F_2^p from NMC [19]. For display purposes F_2^p has been multiplied by the numbers in brackets. The solid and dashed lines correspond to the value of parameters for Fit 1 and 1a, respectively (see text). This notation is hereafter adopted.

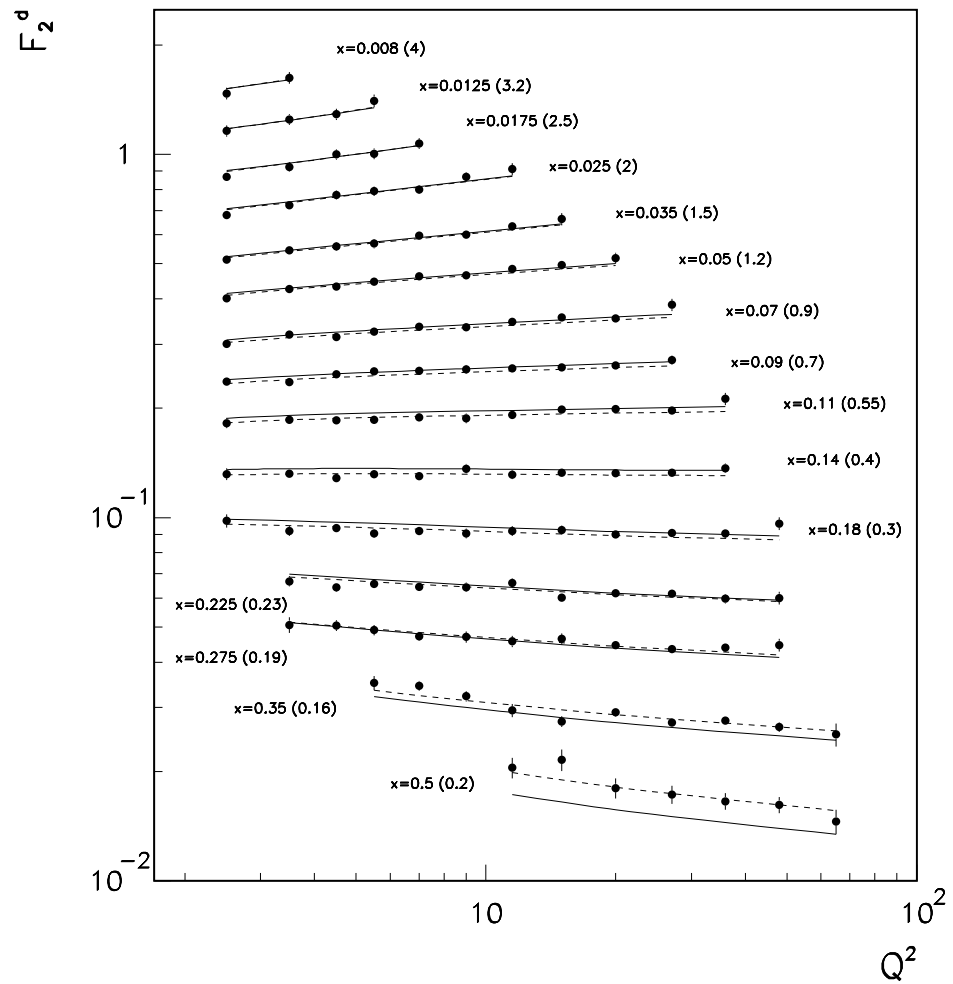


Figure 4: Comparison of the prediction of the fit with the experimental data on F_2^d from NMC [19]. For display purposes F_2^d has been multiplied by the numbers in brackets.

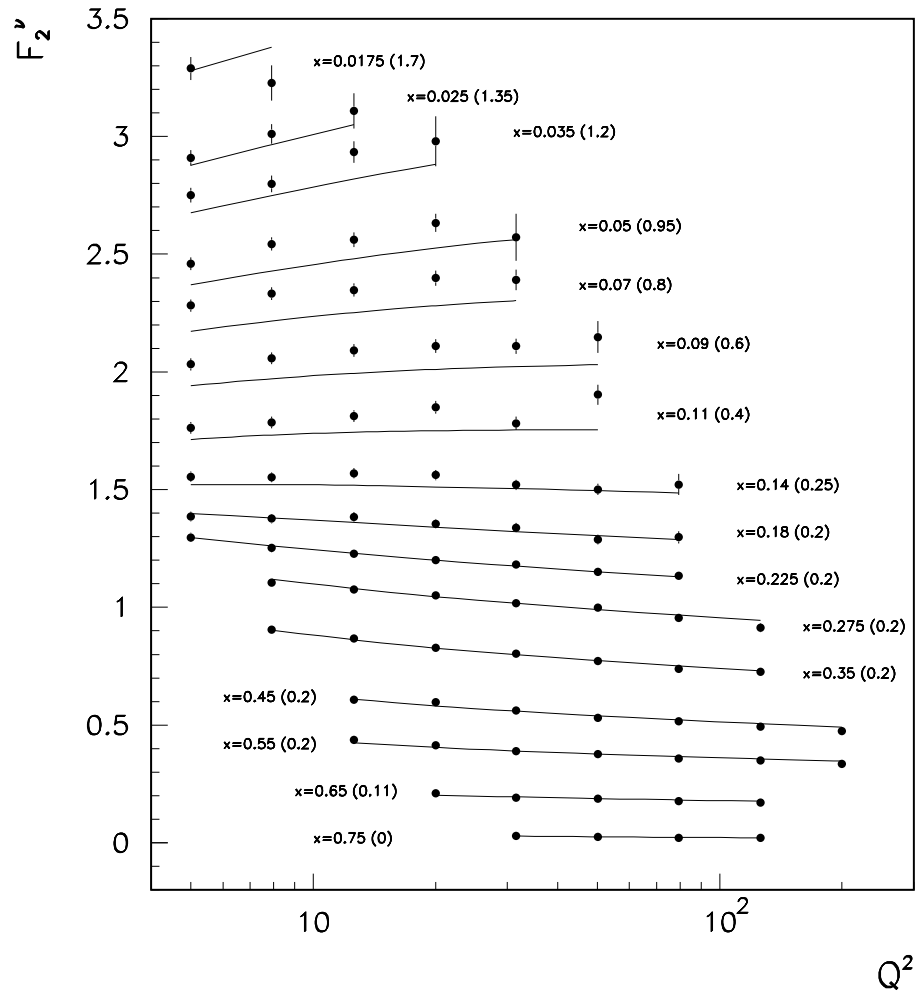


Figure 5: Comparison of the prediction of the fit with the experimental data on F_2^ν from CCFR [7]. For display purposes the numbers in brackets have been added to F_2^ν .

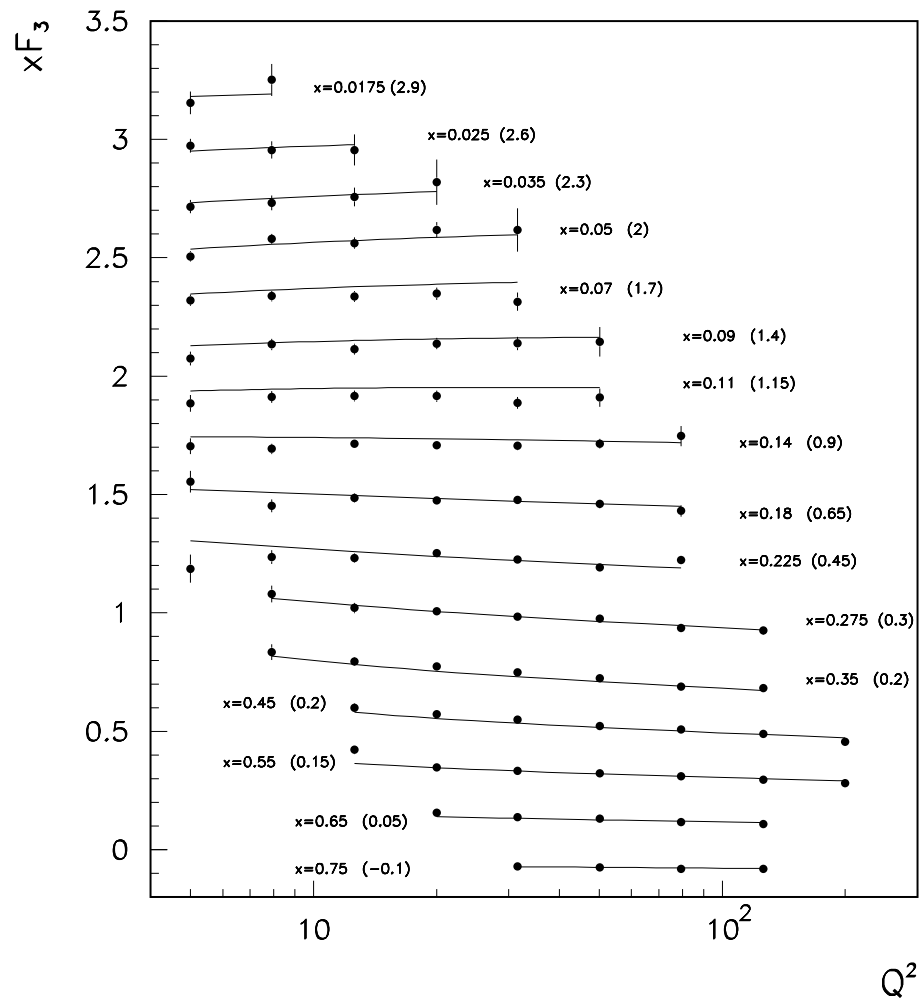


Figure 6: Comparison of the prediction of the fit with the experimental data on $x F_3$ from CCFR [7]. For display purposes the numbers in brackets have been added to $x F_3$.

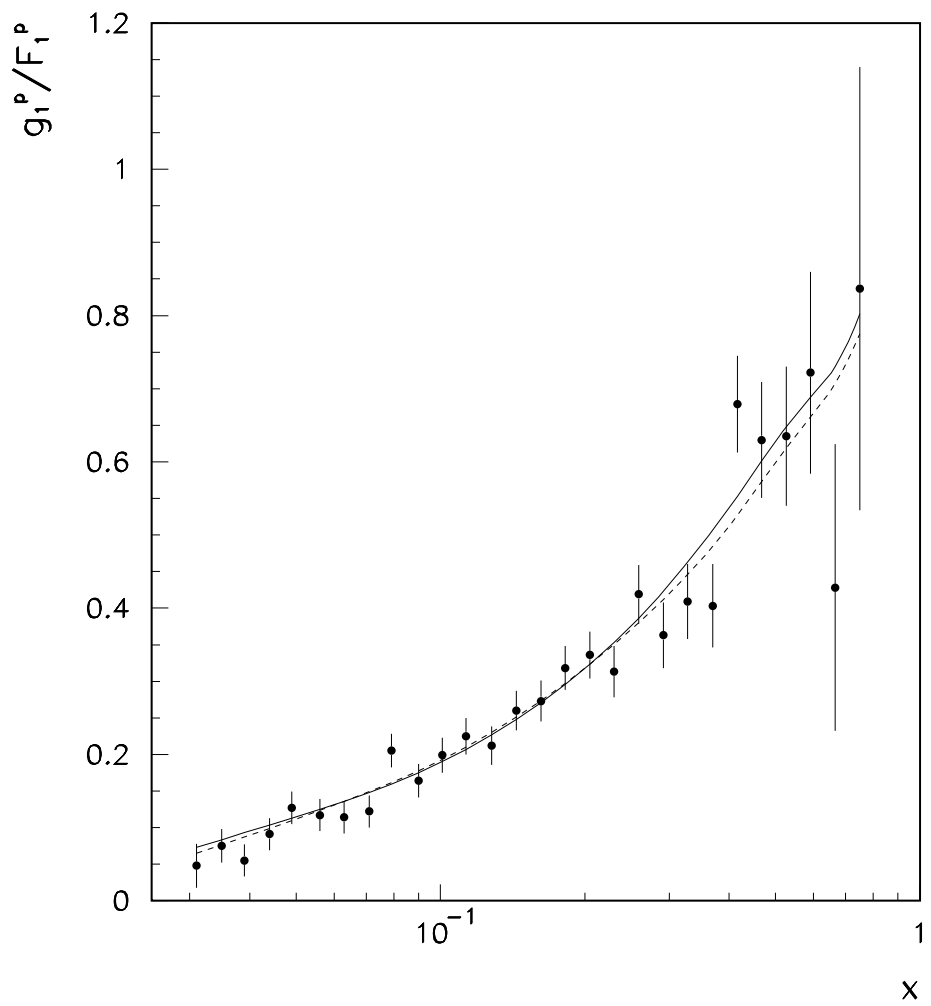


Figure 7: Comparison of the prediction of the fit with the experimental data on g_1^p/F_1^p from E143 [21]. The lines are evaluated at the Q^2 of the experimental points.

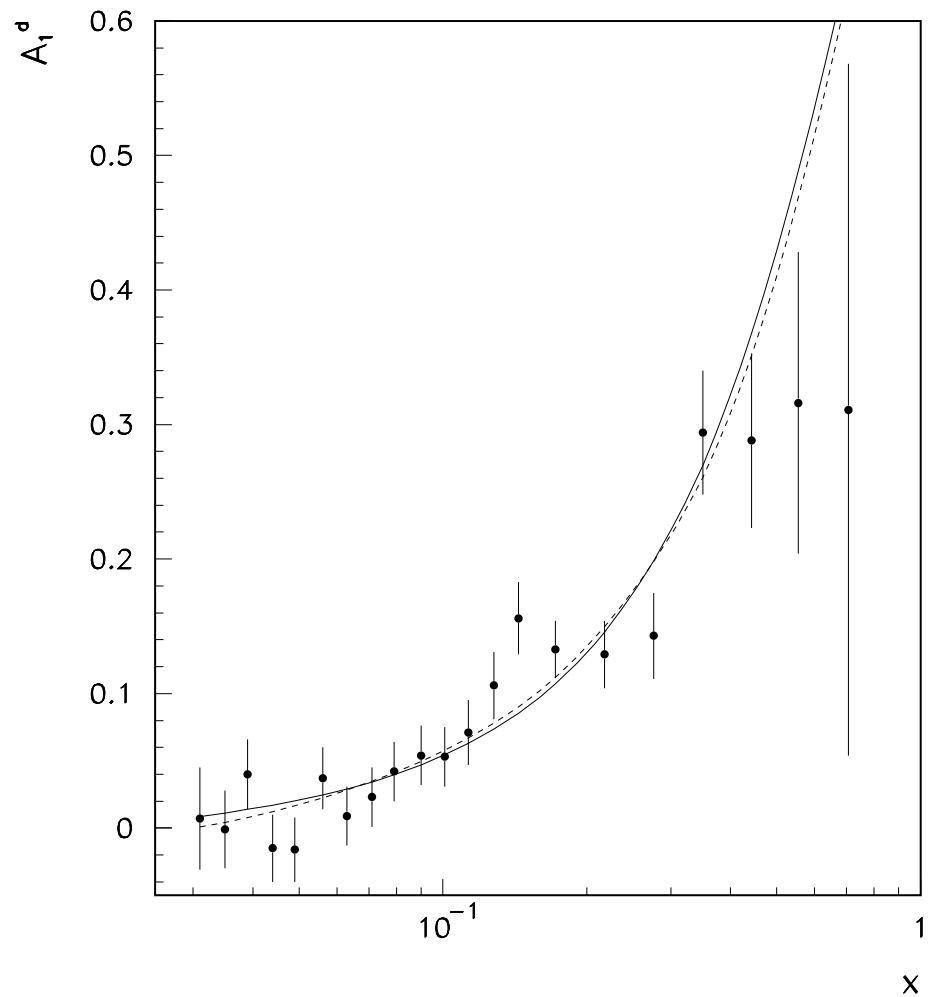


Figure 8: Comparison of the prediction of the fit with the experimental data on A_1^d from E143 [21]. The lines are evaluated at the Q^2 of the experimental points.

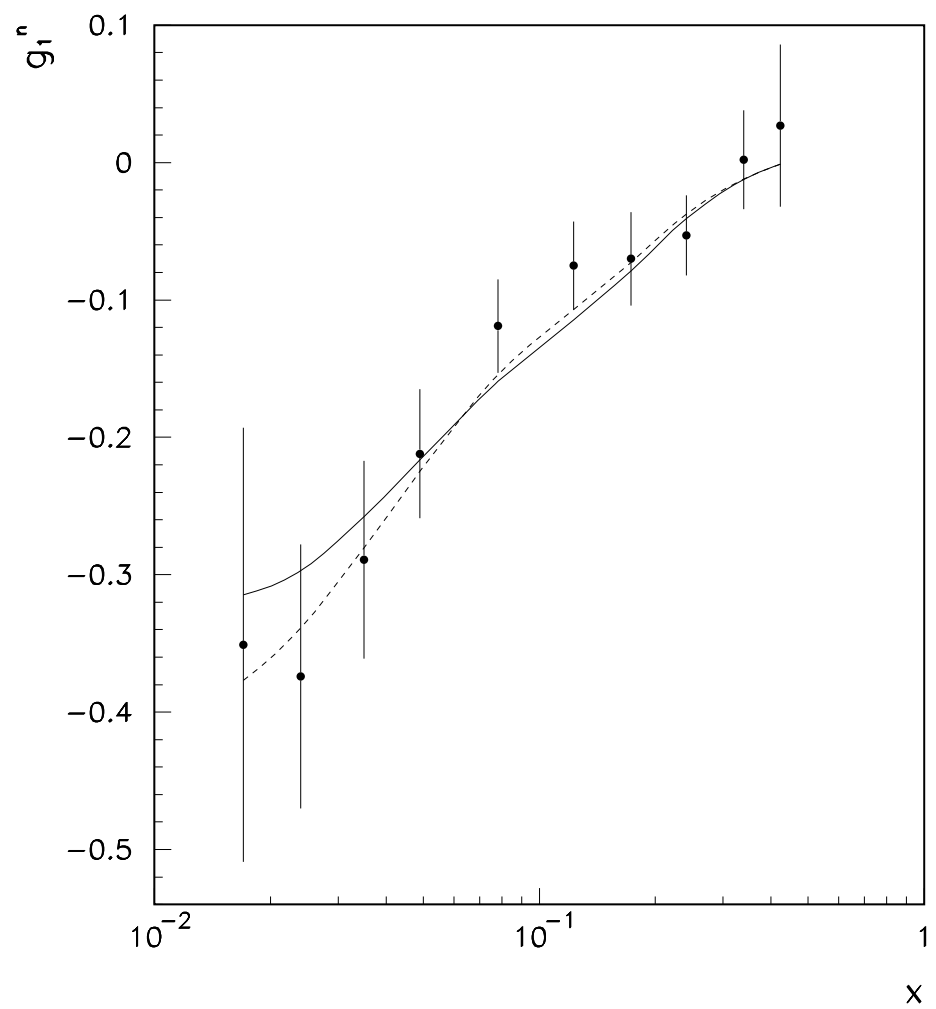


Figure 9: Comparison of the prediction of the fit with the experimental data on g_1^n from E154 [22]. The lines are evaluated at the Q^2 of the experimental points.

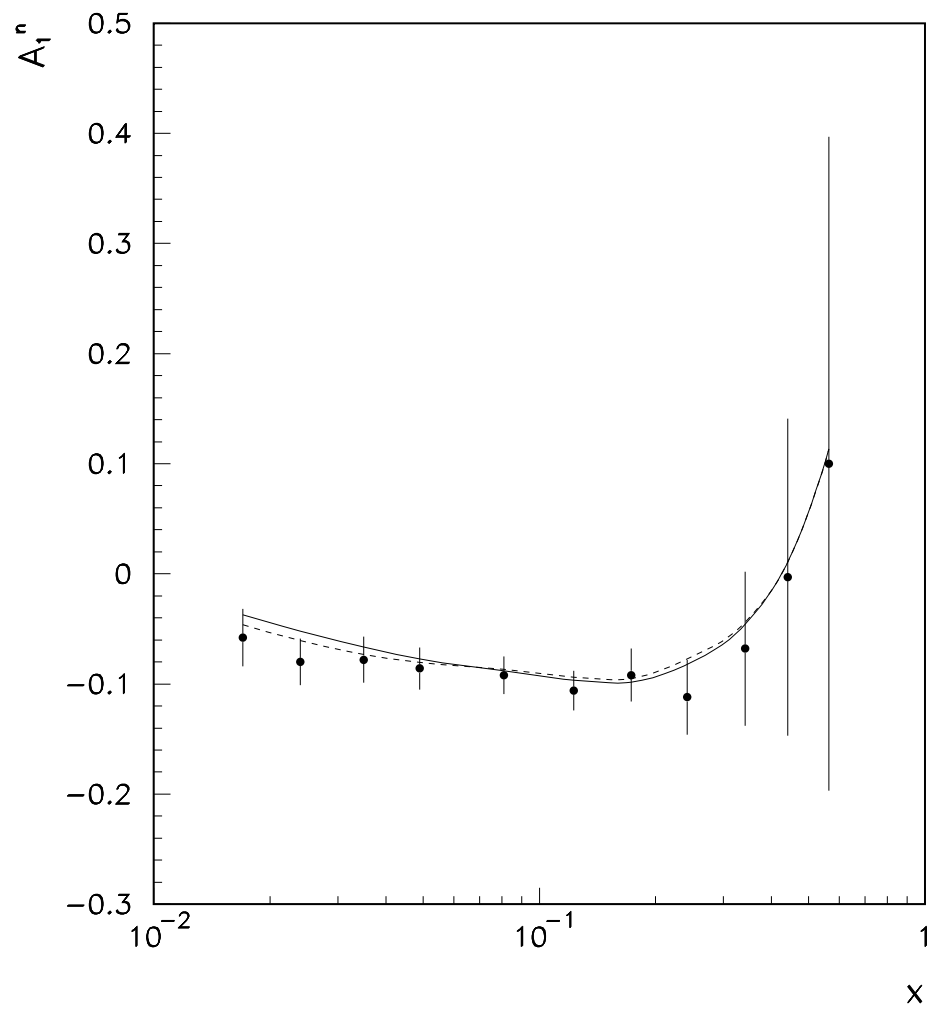


Figure 10: Comparison of the prediction of the fit with the experimental data on A_1^n from E154 [22]. The lines are evaluated at the Q^2 of the experimental points.

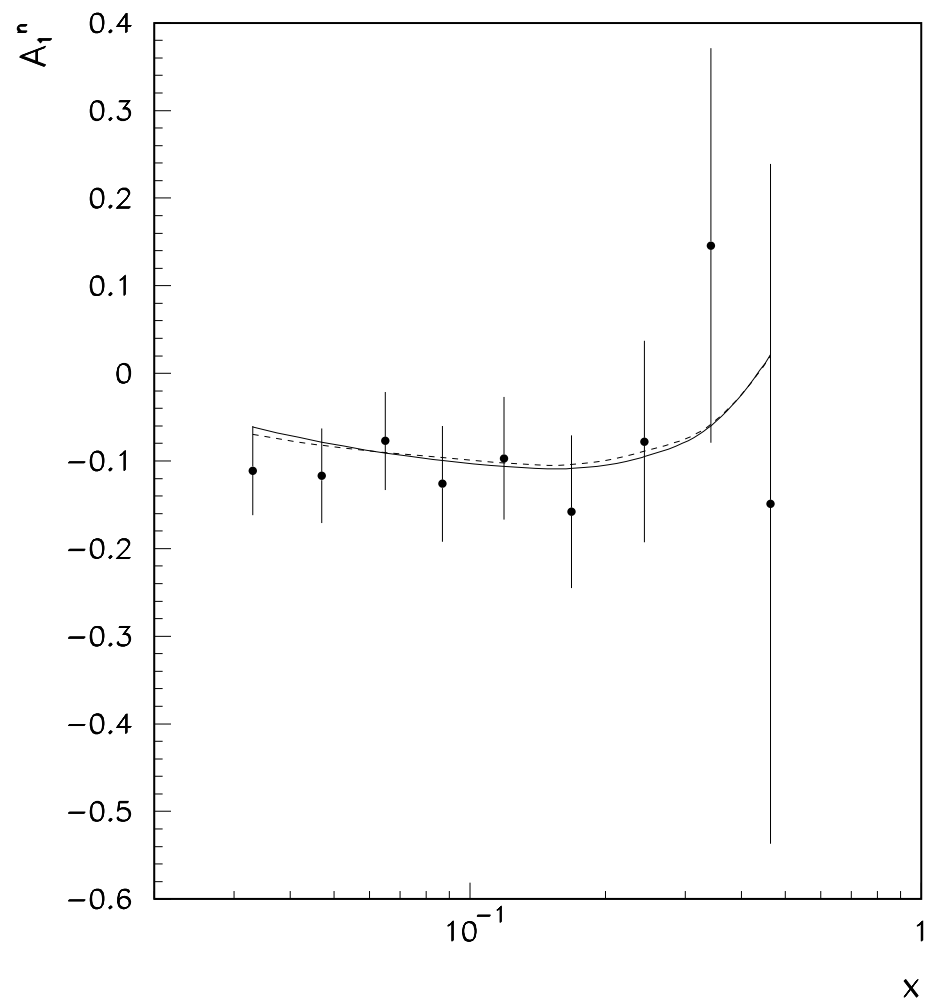


Figure 11: Comparison of the prediction of the fit with the experimental data on A_1^n from HERMES [23]. The lines are evaluated at the Q^2 of the experimental points.

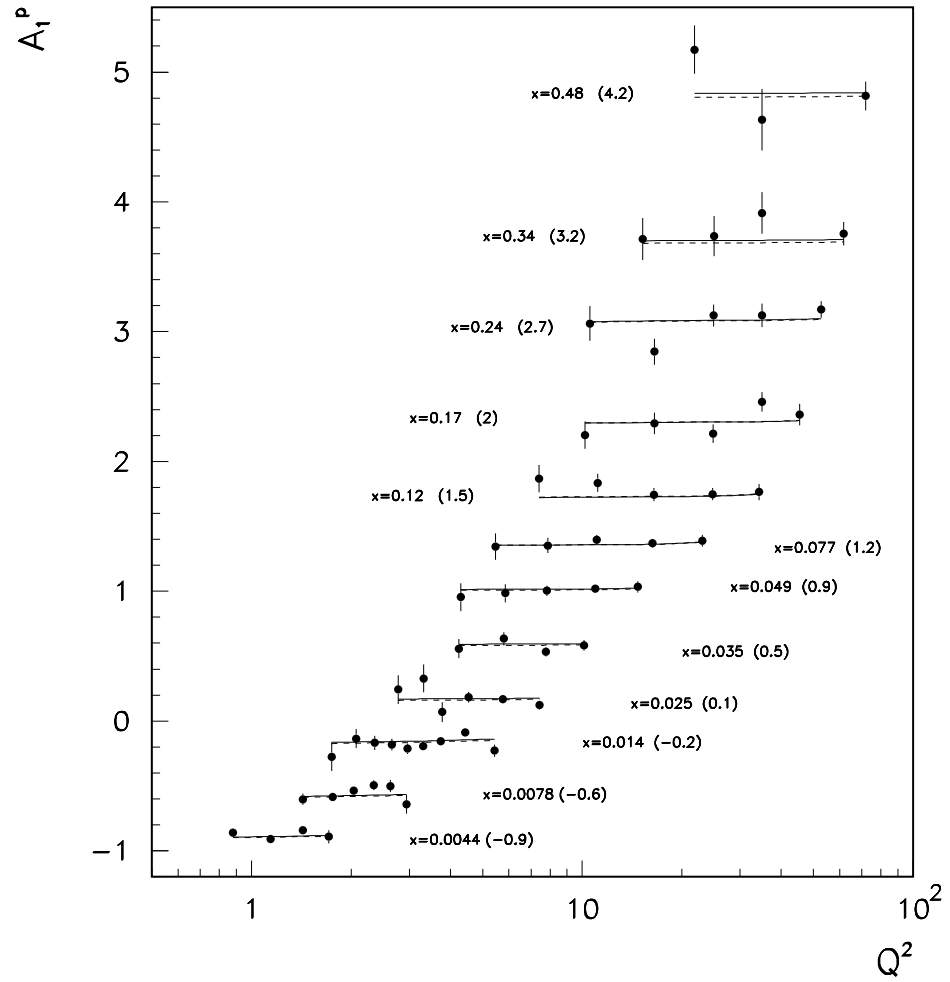


Figure 12: Comparison of the prediction of the fit with the experimental data on A_1^p from SMC [24]. For display purposes data at adjacent x values have been grouped together and the numbers in brackets have been added to A_1^p .

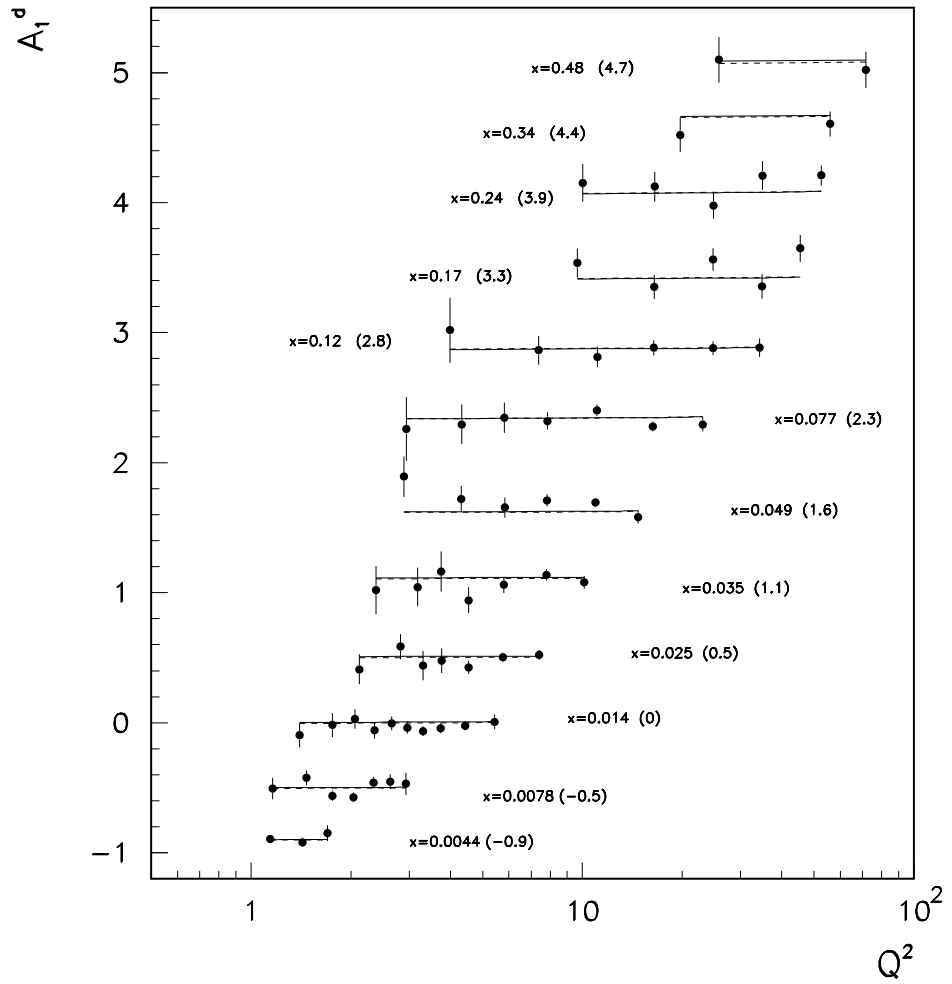


Figure 13: Comparison of the prediction of the fit with the experimental data on A_1^d from SMC [24]. For display purposes data at adjacent x values have been grouped together and the numbers in brackets have been added to A_1^d .